Resonant electrical coupling: circuit model and first experimental results

Ricardo Dias Fernandes, João Nuno Matos and Nuno Borges Carvalho

***Abstract*—The research reported in this article is related to the field of wireless power transfer. In particular, resonant electrical coupling is studied as an alternative to resonant magnetic coupling. Both techniques are analyzed in detail (using circuit models). The strong duality that exists between electrical resonance and magnetic resonance is demonstrated. In terms of experimental validation, the theoretical results are compared with the results obtained with a proof-of-concept prototype. Directions for future research are presented at the end of the article.**

***Index Terms*—Wireless power transfer; resonant electrical coupling; resonant capacitive coupling; resonant coupling; resonant magnetic coupling.**

I. Introduction

THE very first project in the field of wireless power transfer reported in the literature was proposed by Nikola Tesla in 1899. His goal was to build a network of towers that would pump large amounts of energy into the atmospheric layers at moderate altitudes. He was convinced that these layers and the planet would behave as good electrical conductors and wanted to prove that it would be possible to use them to transfer energy over any distance. It would then be possible to collect this accumulated energy from anywhere in the planet, wirelessly. Tesla managed to secure the necessary funding to begin the construction of the first of these towers in 1901. The Wardenclyffe tower was an impressive structure composed by a very large coil wound around a 60 m mast with a 1 m diameter copper ball placed at the top. Also impressive were the 300 kW supplied to the tower at 150 kHz (the resonant frequency of the coil) and the electric potential produced at the sphere, which was around 10^8 V (according to Tesla himself). According to the reports of the journalists of that time, Tesla managed to light up 200 50 W incandescent lamps located 42 km away from the tower [1]. Despite the encouraging results the lack of funding brought the project to a halt (still before the construction was completed) and a few years later, in 1917, the tower was demolished. The principle of operation behind the Wardenclyffe tower relied on concepts still widely used today such as oscillating voltages and currents, capacitor charging and discharging, magnetic induction and resonators [2].

This work was funded by national funds through the FCT - Fundação para a Ciência e a Tecnologia (grant SFRH/BD/69392/2010 and project EXCL/EEI-TEL/0067/2012 - CREATION) and also by the COST action IC1301 WiPE - Wireless power transmission for sustainable electronics.

The authors are with the Instituto de Telecomunicações and Departamento de Electrónica, Telecomunicações e Informática, Universidade de Aveiro, 3810-193, Aveiro, Portugal; the e-mail addresses of the authors are (by order of appearance) rdf@ua.pt, matos@ua.pt and nbcarvalho@ua.pt.

The severe lack of financial resources which caused the failure of the Wardenclyffe project was largely due to the significant advancements in the field of wireless communications, in particular long range. As a result, investors shifted from power to communications, and so did research. Wireless power was only brought back in the 1960s by William C. Brown. Brown conducted several experiments with 2.45 GHz microwave tubes and was the first to coin the term rectenna (a rectenna is an antenna especially designed for receiving and rectifying microwaves). One of his main accomplishments took place at the Jet Propulsion Laboratory, California, in 1975. He was able to transmit 30 kW from a parabolic antenna with a diameter of 26 m to a 3.4 by 7.2 m rectenna placed 1.6 km away. The maximum efficiency achieved was 82.5% (rectification only) obtained at 2.388 GHz and the power transmitted by the parabolic antenna was 450 kW. Prior to this demonstration Brown had already been involved in several other smaller projects related to the same topic. In 1964 he succeeded in transmitting power wirelessly to a tethered helicopter, and 4 years later to a free-flying version (both at 2.45 GHz). In 1975 he was able to transmit 495 W with a total DC-to-DC efficiency of 54%. Although successful, these experiments were expensive and in most cases too large for any practical applications [3]. In addition, most microwave wireless power systems (including those just mentioned) are sensitive to alignment imperfections, which is a consequence of the use of directional antennas. Directional antennas help to increase efficiency if the alignment is correct but otherwise tend to be worse than an isotropic radiator.

A. Resonant magnetic coupling

Not many years ago, in 2007, a group of researchers proposed a novel and very innovative wireless power technology which combines the concepts of inductive coupling and magnetic resonance in a very effective way (and hence the name). Resonant magnetic coupling takes advantage of the fact that the magnetic field between two coils increases significantly if the coils have very high Qs (quality factors) and are designed to resonate at the same frequency. From this discovery resulted several publications of great scientific and industrial importance [4]–[7]. Resonant magnetic coupling was first demonstrated using a system based on the diagram presented in figure 1, which consists of two single-turn coils and two helical coils. In the original prototype the copper wires used to build the coils had a cross-sectional diameter of 6 mm (a rather large value in order to minimize losses). The outer diameter of the multi-turn coils was 60 cm (not exactly small

Fig. 1. Diagram of resonant magnetic coupling, composed by two single-turn coils and two high Q helical coils.

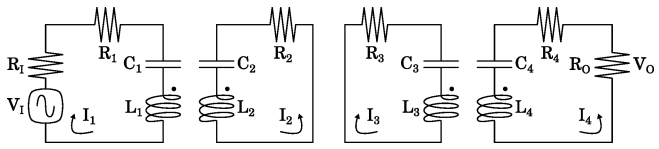

Fig. 2. Circuit model most commonly used to describe resonant magnetic coupling.

but reasonable). Using this system the researchers were able to light up a 60 W incandescent light bulb placed 2 meters away. More importantly, they managed to do so with an efficiency of 40%. An extremely surprising result, especially given the fact that it was obtained with such a simple apparatus. The attention given to this demonstration by the media was quite remarkable. It was the first time that a wireless power system achieved such a balanced trade-off between critical features such as efficiency, range, simplicity, size and power transfer capability.

Resonant magnetic coupling will now be analyzed mathematically based on the circuit model illustrated in figure 2. Even though relatively simple, this model is quite accurate and easy to understand. This is also the model which is most widely used in the literature [8]–[10] (as a note, resonant magnetic coupling was originally described using coupled-mode theory, not a circuit model). The following analysis will be useful later in the article for comparison purposes. Matching the circuit model to the diagram of figure 1 is straightforward since each loop in the circuit corresponds to a coil in the diagram. In terms of circuit elements, R_1, R_2, R_3, R_4, C_2 and C_3 are all parasitic elements. C_1 and C_4 are actual capacitors added to the single-turn coils to ensure that they resonate at the same frequency of the helical coils. R_I and R_O represent the source and load resistances, respectively, and V_I is the input voltage. As for magnetic couplings, L_1 is coupled to L_2, L_2 is coupled to L_3 and L_3 is coupled to L_4. Using M to represent mutual inductance and j as the imaginary unit it is possible to write

$$V_I = I_1(R_I + R_1 - j/(wC_1) + jwL_1) + jwI_2M_{12} \quad (1)$$

$$0 = I_2(R_2 - j/(wC_2) + jwL_2) + jwI_1M_{12} + jwI_3M_{23} \quad (2)$$

$$0 = I_3(R_3 - j/(wC_3) + jwL_3) + jwI_2M_{23} + jwI_4M_{34} \quad (3)$$

$$0 = I_4(R_O + R_4 - j/(wC_4) + jwL_4) + jwI_3M_{34} \quad (4)$$

$$V_O = -I_4R_O. \quad (5)$$

The voltage gain can then be calculated as

$$V_O/V_I = -jw^3M_{12}M_{23}M_{34}R_O/(M_{12}^2M_{34}^2w^4 + Z_1Z_2Z_3Z_4 + w^2(M_{12}^2Z_3Z_4 + M_{23}^2Z_1Z_4 + M_{34}^2Z_1Z_2)), \quad (6)$$

with Z_1, Z_2, Z_3 and Z_4 given by

$$Z_1 = R_I + R_1 - j/wC_1 + jwL_1 \quad (7)$$

$$Z_2 = R_2 - j/wC_2 + jwL_2 \quad (8)$$

$$Z_3 = R_3 - j/wC_3 + jwL_3 \quad (9)$$

$$Z_4 = R_O + R_4 - j/wC_4 + jwL_4. \quad (10)$$

In addition, M_{12}, M_{23} and M_{34} can be written as a function of magnetic coupling coefficients

$$M_{12} = k_{12}\sqrt{L_1L_2}, 0 \leq k_{12} \leq 1 \quad (11)$$

$$M_{23} = k_{23}\sqrt{L_2L_3}, 0 \leq k_{23} \leq 1 \quad (12)$$

$$M_{34} = k_{34}\sqrt{L_3L_4}, 0 \leq k_{34} \leq 1. \quad (13)$$

Since the power delivered to R_O is

$$P_O = |V_O|^2/(2R_O) \quad (14)$$

and the power source (V_I plus R_I) is able to supply at most (considering a matched load)

$$P_A = |V_I|^2/(8R_I), \quad (15)$$

the available power gain can be written as a function of the voltage gain previously calculated in (6) as

$$P_O/P_A = 4R_I|V_O/V_I|^2/R_O. \quad (16)$$

In this part the available power gain will now be calculated for several k_{23} values considering the parameters listed in table I. Figure 3 illustrates the response of the model as a function of frequency for k_{23} between 0.001 and 0.015. It can be seen in the figure that the higher the k_{23} the better the response. For k_{23} equal to 0.001 the gain is still below the 2% mark. This is not surprising since 0.001 is very close to zero and in theory if k_{23} is zero then (12) is zero, (6) is zero and (16) is also zero. The gain however increases rather quickly as k_{23} is increased. For k_{23} equal to 0.015 (which is still clearly a small value) the gain is already 53%. Another important aspect about this figure is that the gain is maximum always at the same frequency, regardless of the k_{23} considered. This is the frequency at which the circuit resonates and can be estimated using

$$f_r = 1/\left(2\pi\sqrt{L_iC_i}\right), \quad (17)$$

with i equal to 1, 2, 3 or 4 (since all the coils were designed to resonate at the same frequency the product L_iC_i must be always the same). In figure 4 the response of the model is shown for values of k_{23} between 0.02 and 0.1. The most remarkable aspect in this figure is the frequency splitting. For k_{23} equal to 0.026 and higher it is possible to observe two distinct resonant frequencies instead of one. Also important is the fact that the peak gain is 58% for k_{23} equal to 0.02 just before the splitting occurs and 60% at the highest k_{23} which means that the gain does not change much during this phase. On the other hand, the spacing between the resonant frequencies increases considerably. For instance, when k_{23} is equal to 0.1 the resonant frequencies are separated by

TABLE I
PARAMETERS USED IN THE ANALYSIS OF THE CIRCUIT MODEL PRESENTED IN FIGURE 2.

Parameter	Value
R_I, R_O	50 Ω
R_1, R_4	2 Ω
R_2, R_3	10 Ω
L_1, L_4	1 μH
L_2, L_3	28 μH
C_1, C_4	140 pF
C_2, C_3	5 pF
k_{12}, k_{34}	0.1

approximately 2.8 MHz. Figure 5 illustrates the response of the model using a different perspective. It is possible to see in this figure that the splitting is almost symmetrical (not entirely symmetrical only due to the difference in the peaks visible in figure 4).

So far the parameters k_{12} and k_{34} were considered both constant and equal to 0.1. Theoretically, if k_{12} is zero then (11) is zero, (16) is zero and (16) is also zero. Similarly, if k_{34} is zero then (13) is zero, (16) is zero and (16) is also zero. The lower gain presented in figure 6 as a result of reducing k_{12} and k_{34} to 0.09 is therefore not surprising. In this case the gain decreases from 60% to 55%. On the other hand, if k_{12} and k_{34} are increased the gain increases (as would be reasonable to expect), but only for the higher k_{23} values. For instance, in figure 7 k_{12} and k_{34} are equal to 0.18 and compared to figure 4 the gain increases for k_{23} equal to 0.038, 0.06 and 0.1 and decreases for k_{23} equal to 0.02 and 0.026. In the highest k_{23} the improvement is from 60% to 80% and in the lowest k_{23} the gain drops from 58% to 30%. Clearly, the optimal values of k_{12} and k_{34} change depending on which k_{23} is considered [8]. In conclusion, 0.1 is a reasonable choice for k_{12} and k_{34} given the circuit elements selected.

II. RESONANT ELECTRICAL COUPLING

For the analysis of resonant electrical coupling the circuit model illustrated in figure 8 will be considered. As before, V_I and R_I represent the source and R_O the load. In this circuit model L_1 and L_2 are not magnetically coupled which means that the source and the load are connected only through C_3 and C_4. The losses in L_1 and L_2 are accounted for by R_1 and R_2, respectively. Considering C_3 and C_4 as an admittance two-port network it is possible to write

$$Y_{11} = jwC_3C_4/(C_3 + C_4) \quad (18)$$
$$Y_{12} = -Y_{11} \quad (19)$$
$$Y_{21} = -Y_{11} \quad (20)$$
$$Y_{22} = Y_{11} \quad (21)$$

and also

$$V_I = I_3(R_I + R_1 - j/(wC_1) + jwL_1) - jI_1/(wC_1) \quad (22)$$
$$0 = I_4(R_O + R_2 - j/(wC_2) + jwL_2) + jI_2/(wC_2) \quad (23)$$
$$V_O = I_4R_O \quad (24)$$
$$I_1 = Y_{11}V_1 + Y_{12}V_2 \quad (25)$$
$$I_2 = Y_{21}V_1 + Y_{22}V_2. \quad (26)$$

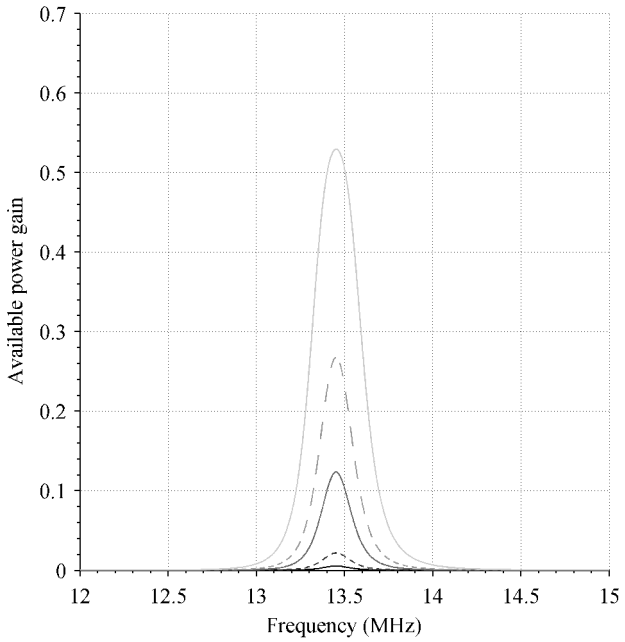

Fig. 3. Available power gain as a function of frequency for k_{23} equal to 0.001 (dark gray), 0.002, 0.005, 0.008 and 0.015 (light gray).

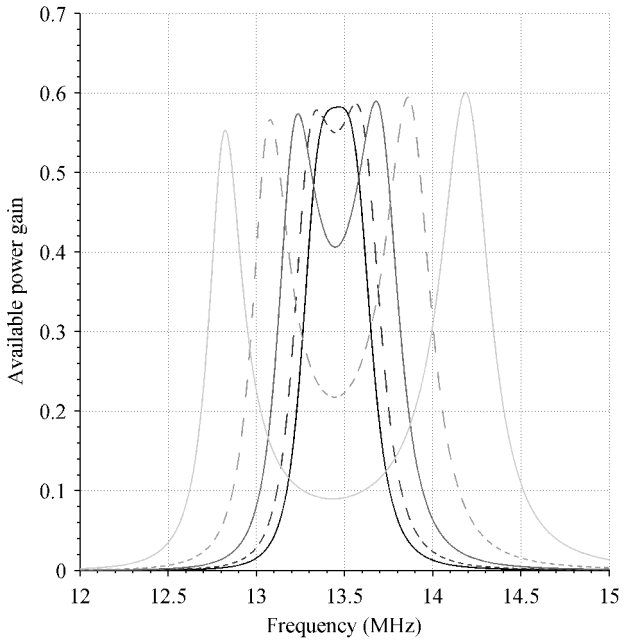

Fig. 4. Available power gain as a function of frequency for k_{23} equal to 0.02 (dark gray), 0.026, 0.038, 0.06 and 0.1 (light gray).

The voltage gain can be expressed as

$$V_O/V_I = R_O(Y_{12} - (Y_{11} + jwC_1 + 1/Z_1)(Y_{22} + jwC_2 + 1/Z_2)/Y_{21})^{-1}/(Z_1Z_2), \quad (27)$$

with Z_1 and Z_2 are given by

$$Z_1 = R_I + R_1 + jwL_1 \quad (28)$$

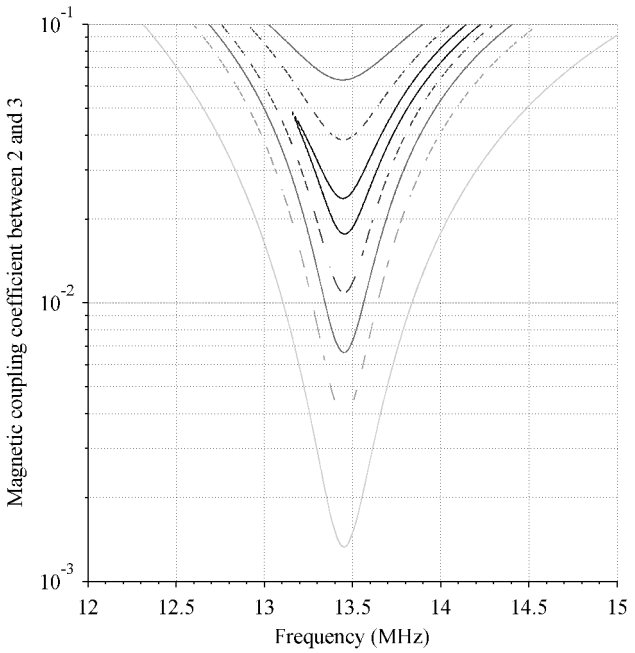

Fig. 5. Available power gain as a function of frequency and k_{23} using contour lines drawn at 0.01 (light gray), 0.08, 0.2, 0.4 and 0.57 (dark gray).

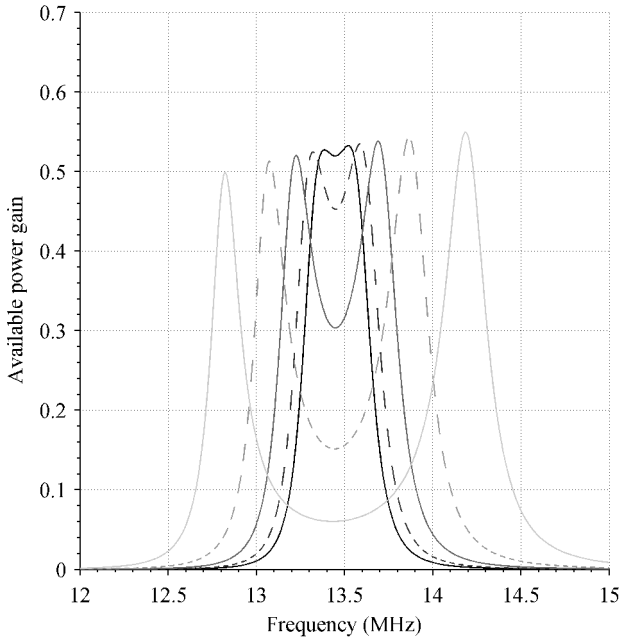

Fig. 6. Available power gain as a function of frequency for k_{23} equal to 0.02 (dark gray), 0.026, 0.038, 0.06 and 0.1 (light gray) with k_{12} and k_{34} reduced to 0.09.

$$Z_2 = R_O + R_2 + jwL_2. \tag{29}$$

It is important to note that it would be perfectly possible to obtain the voltage gain without a two-port network. The purpose of this approach will be explained later. From (27) the available power gain can be calculated using (16).

Following the same procedure as before, a concrete realization of the circuit model will now be considered. The parameters selected for this analysis are listed in table II (they are similar to the parameters used before in order to allow a fair comparison with resonant magnetic coupling). In addition, in this analysis it will be always assumed that

$$C_4 = C_3. \tag{30}$$

For C_3 between 0.02 and 0.18 pF the response of the model can be seen in figure 9. In theory, if C_3 is zero then C_4 is zero, which makes all of the admittance parameters tend to zero. As a consequence, (27) and (16) tend to zero as well. The very small gain for the lowest C_3 is therefore not surprising. The gain increases considerably as C_3 is increased and reaches 55% for C_3 equal to 0.18 pF. The frequency at which the system resonates decreases slightly as C_3 is increased but other than the response is similar to figure 3. As before, the resonant frequency can be estimated using (17). In figure 10 the response of the model is shown for values of C_3 between 0.22 and 1 pF. In this figure, as in figure 4, the resonant frequency also splits into two at a certain point. In this figure, as in figure 4, after the splitting occurs the gain also stabilizes and the spacing between the resonant frequencies also increases. In this case, however, the splitting is very asymmetrical, with the upper resonance barely moving. A different view of the frequency splitting, comparable to figure 5, is presented in figure 11.

For the same L_iC_i product in (17) the response of the model can change very substantially. For instance, if L_1 and L_2 are doubled and C_1 and C_2 are reduced to half the gain improves as illustrated in figure 12. Compared to figure 9 the gain increases considerably faster and for C_3 equal to 0.1 pF

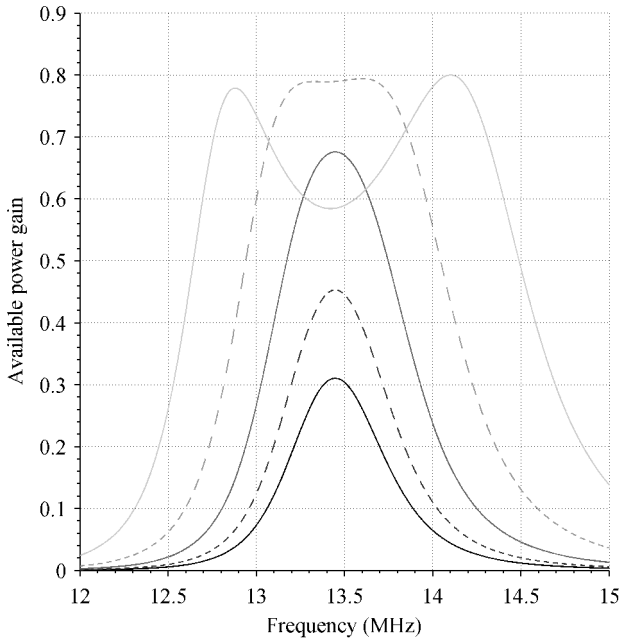

Fig. 7. Available power gain as a function of frequency for k_{23} equal to 0.02 (dark gray), 0.026, 0.038, 0.06 and 0.1 (light gray) with k_{12} and k_{34} increased to 0.18.

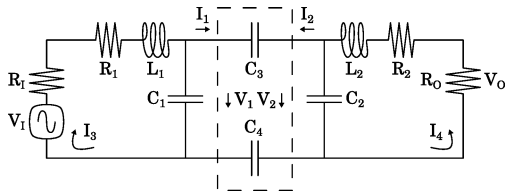

Fig. 8. Circuit model considered in the theoretical study of resonant electrical coupling.

TABLE II
PARAMETERS USED IN THE ANALYSIS OF THE CIRCUIT MODEL PRESENTED IN FIGURE 8.

Parameter	Value
R_I, R_O	50 Ω
R_1, R_2	12 Ω
L_1, L_2	28 μH
C_1, C_2	5 pF

the resonant frequency is already split into two. As for peak value, there are absolutely no changes from to figure 10. The disadvantage is that in this case an inductor with twice the value and the same parasitic resistance is required. In contrast, as shown in figure 13, if the capacitors are doubled and the inductors reduced to half the gain drops to almost nothing.

A. Effect of the parasitic resistances

If R_1 and R_2 are reduced to zero the response of the model improves in a very significant fashion, as shown in figure 14. The improvement is both in terms of rate of increase and, very importantly, peak value. For C_3 equal to 0.18 pF the gain is already above the 95% mark, something that is significantly better than the 55% obtained in figure 10. For C_3 equal to 0.22 pF and higher it can be seen in figure 15 that the gain reaches 100%. In conclusion, the higher the Q of the coils the higher the maximum gain. In the case of resonant magnetic coupling, if R_1, R_2, R_3 and R_4 are reduced to zero the improvement is very similar. For k_{23} equal to 0.015 the gain is already above 95%, as shown in figure 16. It reaches 100% for k_{23} equal to 0.02 or higher at both resonant frequencies, as can be seen in figure 17.

B. Mismatch sensitivity

Figure 18 illustrates how the response of the model is affected by a mismatch one of the circuit components. In this case L_1 was reduced by 10% without reducing L_2 by the same amount. While not very large, this variation is enough to reduce the gain from the 53% obtained in figure 9 to a mere 7%. Unlike in figure 9, two resonant frequencies can now be seen even at the lowest C_3 value considered. In addition, the spacing between the resonant frequencies is approximately the same for all C_3 values. For higher C_3 values, however, the spacing increases as shown in figure 19. In addition, the gain increases to more acceptable values. For instance, for C_3 equal to 1 pF the gain is about 51%. In the case of resonant magnetic coupling reducing L_2 by 10% also has a negative effect on the response of the model. In figures 20 and 21 it is possible to

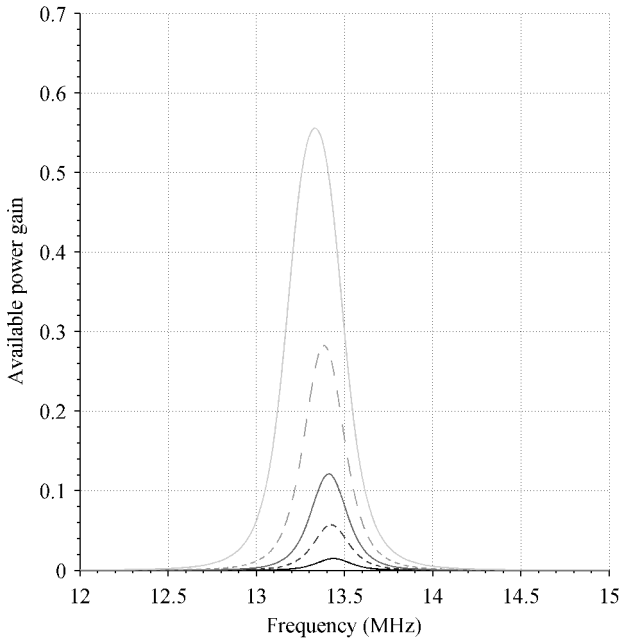

Fig. 9. Available power gain as a function of frequency for C_3 equal to 0.02 (dark gray), 0.04, 0.06, 0.1 and 0.18 pF (light gray).

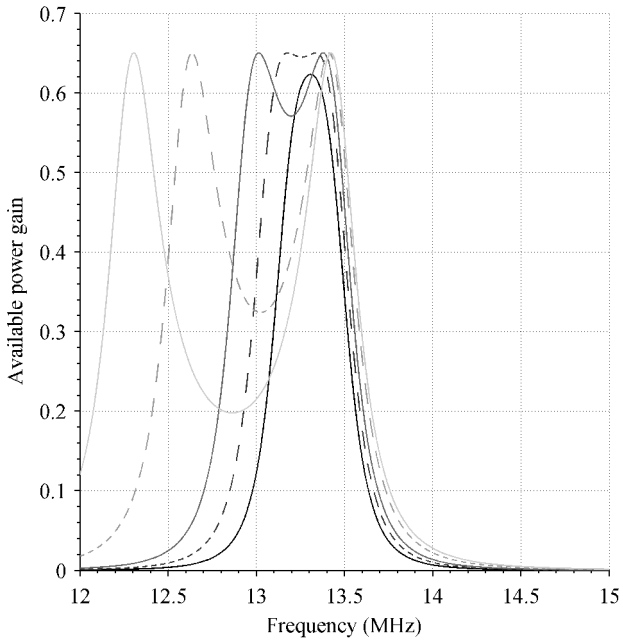

Fig. 10. Available power gain as a function of frequency for C_3 equal to 0.22 (dark gray), 0.3, 0.4, 0.7 and 1 pF (light gray).

see two distinct resonant frequencies even at the lowest k_{23} values and a significant drop in terms of gain compared to 3 and 4, respectively. As can be seen by comparing figure 20 with figure 18 and figure 21 with figure 19, the responses of resonant magnetic coupling and resonant electrical coupling to this non-ideal scenario are remarkably similar.

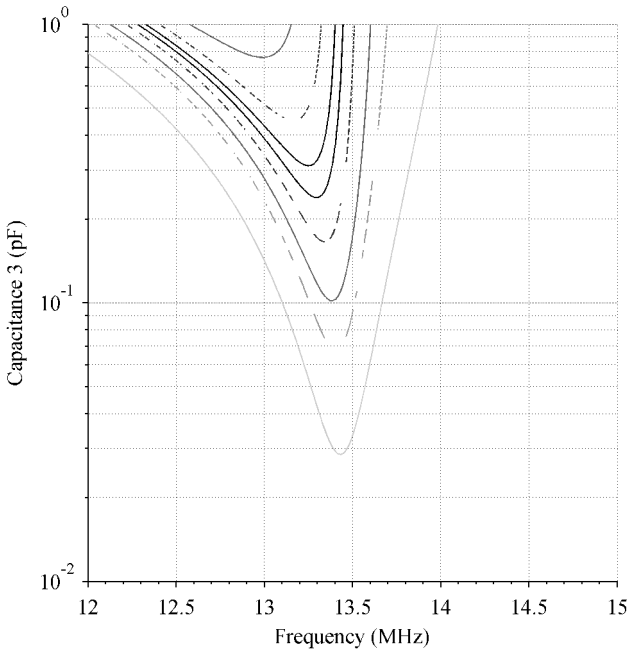

Fig. 11. Available power gain as a function of frequency and C_3 using contour lines drawn at 0.03 (light gray), 0.15, 0.29, 0.52 and 0.64 (dark gray).

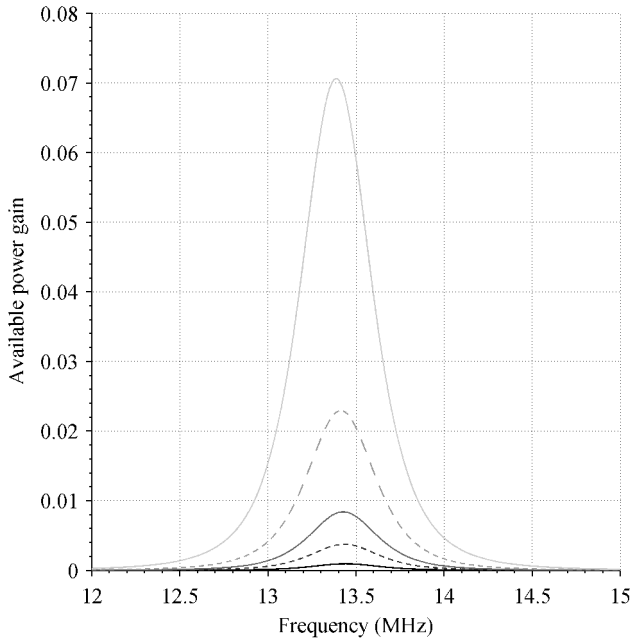

Fig. 13. Available power gain as a function of frequency for C_3 equal to 0.02 (dark gray), 0.04, 0.06, 0.1 and 0.18 pF (light gray) with C_1 and C_2 increased to 10 pF and L_1 and L_2 reduced to 14 μH.

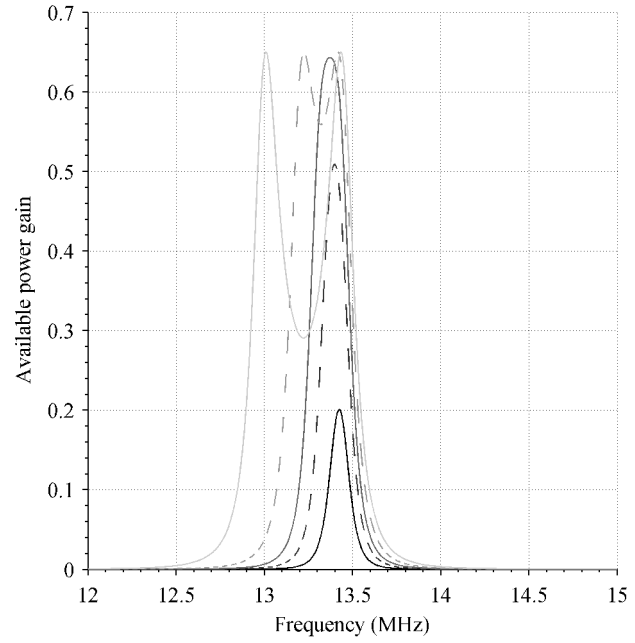

Fig. 12. Available power gain as a function of frequency for C_3 equal to 0.02 (dark gray), 0.04, 0.06, 0.1 and 0.18 pF (light gray) with L_1 and L_2 increased to 56 μH and C_1 and C_2 reduced to 2.5 pF.

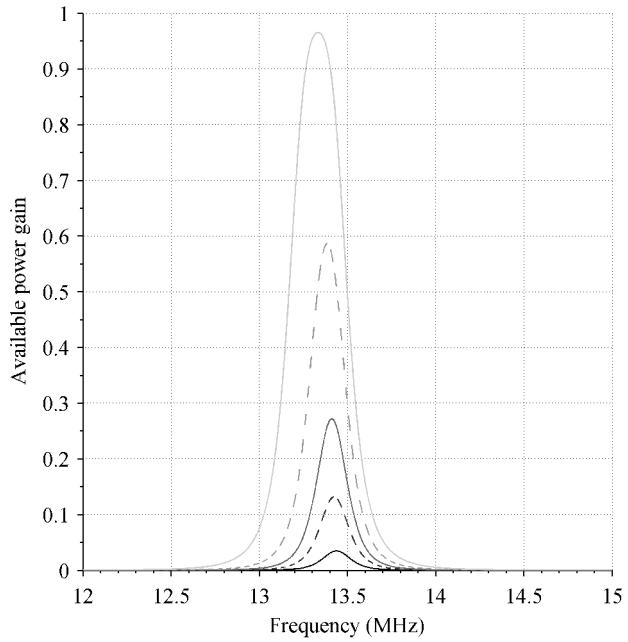

Fig. 14. Available power gain as a function of frequency for C_3 equal to 0.02 (dark gray), 0.04, 0.06, 0.1 and 0.18 pF (light gray) with R_1 and R_2 reduced to zero.

III. Experimental results

A photograph of the prototype designed with the purpose of implementing the circuit model is shown in figure 22. The prototype consists of two mirrored 16 by 16 cm boards made of FR-4, each one with two main copper areas and a helical coil with 40 turns built using 0.8 mm diameter stranded copper wire (stranded wire helps to minimize the parasitic resistance). Each coil has a diameter of 3.6 cm and, as seen in the figure, is located on the back side of the corresponding board. It is important to note that in this prototype C_1 and C_2 are not implemented with actual capacitors but rather taking advantage of the capacitance created between the main copper areas in each

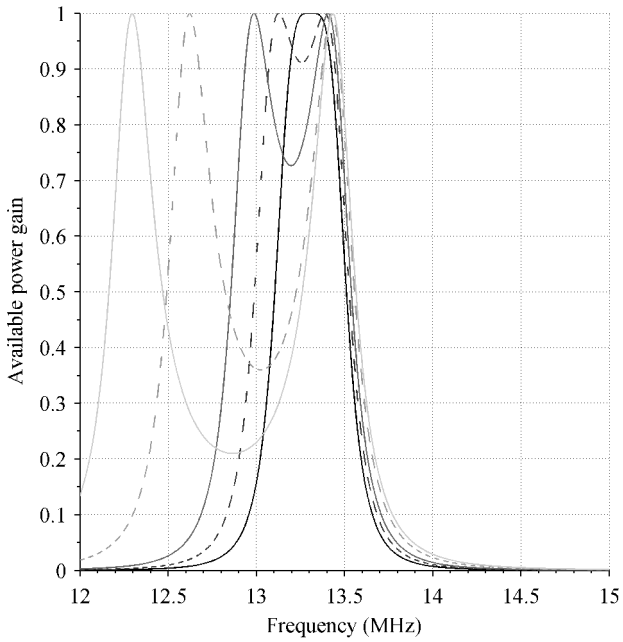

Fig. 15. Available power gain as a function of frequency for C_3 equal to 0.22 (dark gray), 0.3, 0.4, 0.7 and 1 pF (light gray) with R_1 and R_2 reduced to zero.

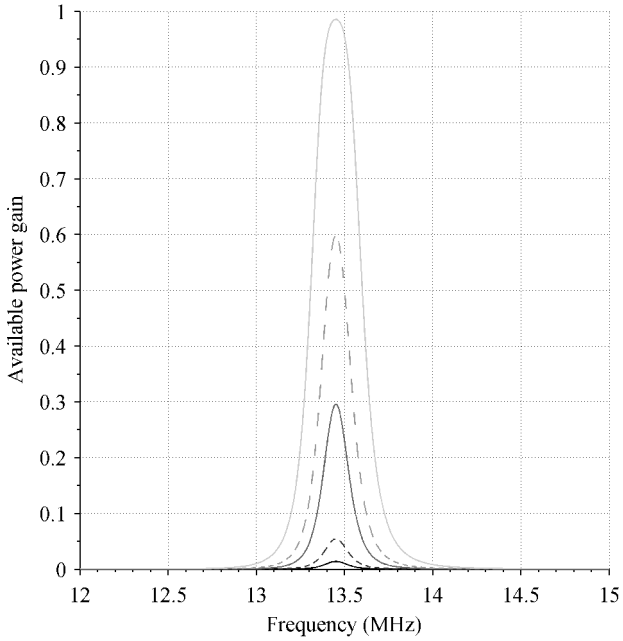

Fig. 16. Available power gain as a function of frequency for k_{23} equal to 0.001 (dark gray), 0.002, 0.005, 0.008 and 0.015 (light gray) with R_1, R_2, R_3 and R_4 reduced to zero.

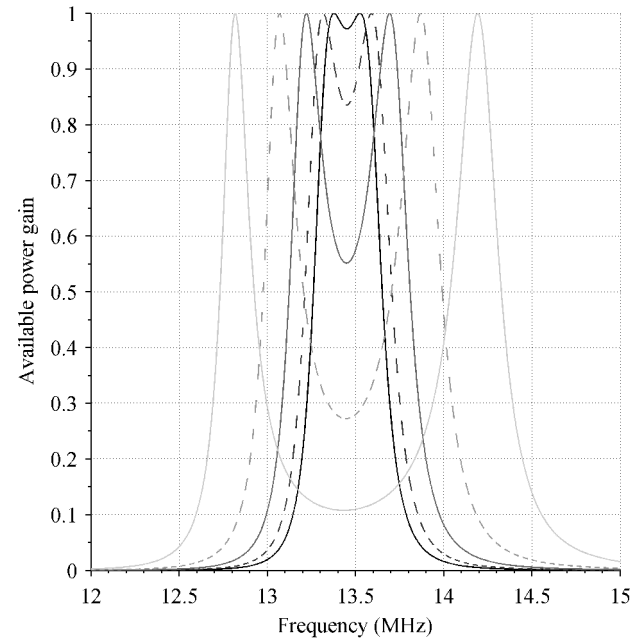

Fig. 17. Available power gain as a function of frequency for k_{23} equal to 0.02 (dark gray), 0.026, 0.038, 0.06 and 0.1 (light gray) with R_1, R_2, R_3 and R_4 reduced to zero.

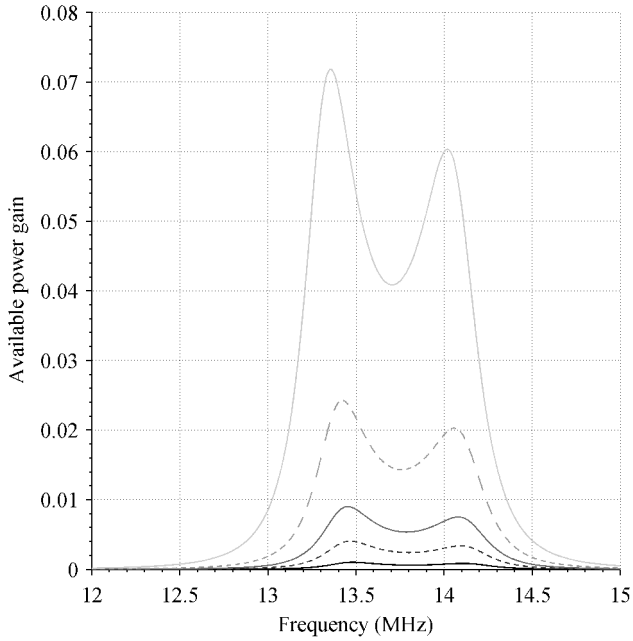

Fig. 18. Available power gain as a function of frequency for C_3 equal to 0.02 (dark gray), 0.04, 0.06, 0.1 and 0.18 pF (light gray) with L_2 reduced to 25.2 μH (-10%).

board. Figure 23 shows the $|S_{21}|$ parameter of the prototype measured at various distances between 10 and 500 cm. These results were obtained with an HP 8753D network analyzer with the prototype mounted on top of polystyrene supports in order to ensure a constant distance of about 1 m to the floor, . One of the most important aspects in figure 23 is that a resonant behavior can be effectively observed in practice. For smaller distances (which correspond to higher C_3 values in the model) two different resonant frequencies can be observed. As the distance is increased the gap becomes smaller. In addition, the lower resonance seems to move faster than the upper

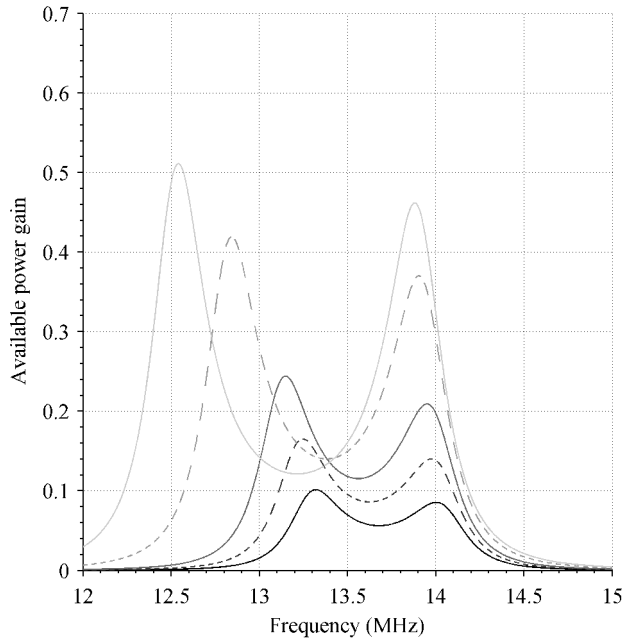

Fig. 19. Available power gain as a function of frequency for C_3 equal to 0.22 (dark gray), 0.3, 0.4, 0.7 and 1 pF (light gray) with L_2 reduced to 25.2 μH (-10%).

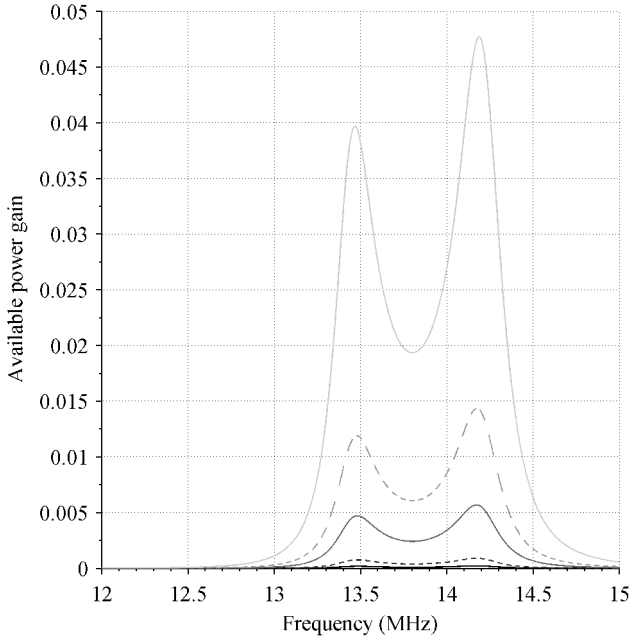

Fig. 20. Available power gain as a function of frequency for k_{23} equal to 0.001 (dark gray), 0.002, 0.005, 0.008 and 0.015 (light gray) with L_3 reduced to 25.2 μH (-10%).

resonance (although the difference is not as significant as in figure 10). While it is very encouraging to see these results match the model there are other results that clearly do not match. For instance, the amplitude of the peaks is not identical. Also, the resonant frequencies do not converge even when the

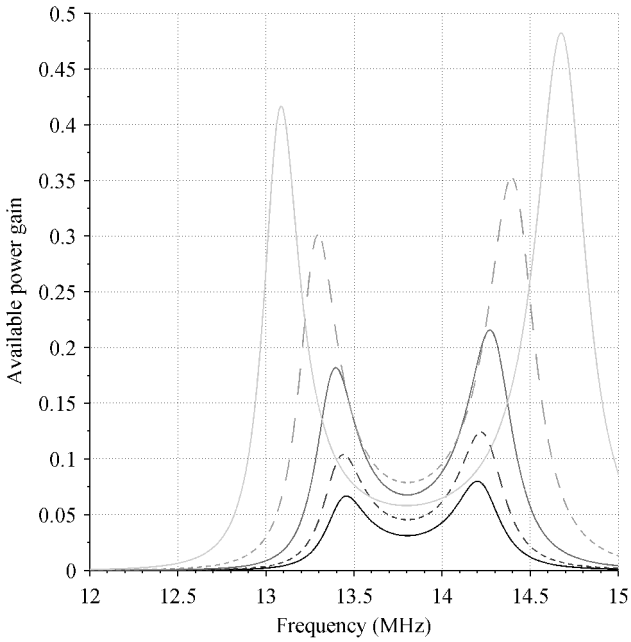

Fig. 21. Available power gain as a function of frequency for k_{23} equal to 0.02 (dark gray), 0.026, 0.038, 0.06 and 0.1 (light gray) with L_3 reduced to 25.2 μH (-10%).

distance is increased to 500 cm (the largest distance available for this test). Moreover, between 90 and 500 cm the difference in $|S_{21}|$ is small. While these aspects were not expected they were observed consistently across several measurements and confirmed on a second network analyzer, an Agilent E8361C. Figure 24 shows the $|S_{12}|$ parameter. As expected, since the devices are identical, the $|S_{21}|$ and $|S_{12}|$ are very similar. Figures 25 and 26 show the $|S_{11}|$ and $|S_{22}|$ parameters. These parameters are not identical in terms of magnitude at each resonant frequency but the locations of the minima are the same. In addition, these minima match the maxima of $|S_{21}|$ and $|S_{12}|$. The maximum $|S_{21}|$ values measured were always in the order of -4 dB. This corresponds to a power gain close to 40% using the well known approximation

$$G \approx |S_{21}|^2. \tag{31}$$

In order to measure the variation of $|S_{21}|$ with angle at a distance of 500 cm the board connected to the second port of the network analyzer was rotated as indicated in figure 27. In figure 28 it can be seen that the $|S_{21}|$ remains quite stable.

A. *Parasitic capacitances*

Depending on how the circuit model is implemented in practice it may be necessary to consider the existance of additional capacitances as shown in figure 29, rather than just C_3 and C_4. These additional capacitances can, however, negatively affect the performance of the model very significantly. For instance, if it is assumed that C_5 and C_6 exist and that

$$C_5 = 0.7C_3 \tag{32}$$

$$C_6 = C_5, \tag{33}$$

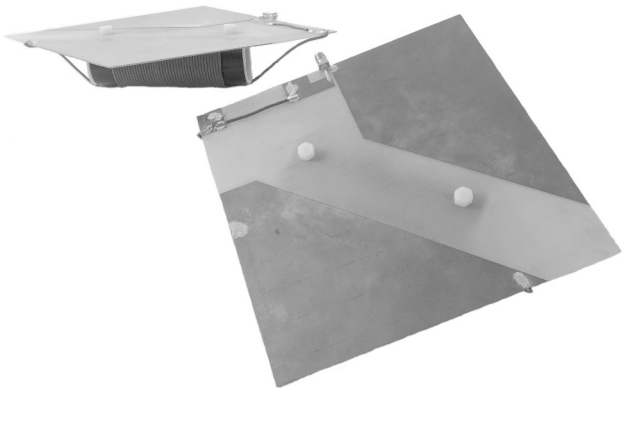

Fig. 22. Photograph of the prototype used to study resonant electrical coupling (based on the model of figure 8).

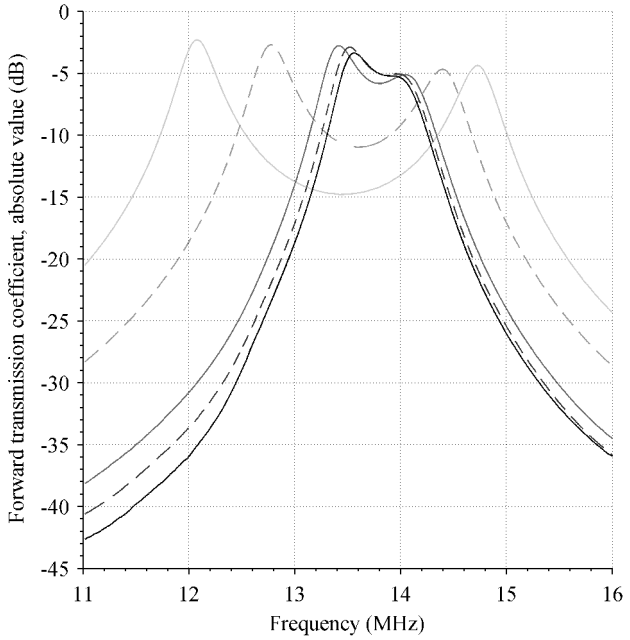

Fig. 23. Measured $|S_{21}|$ as a function of frequency for distances equal to 10 (light gray), 20, 60, 90 and 500 cm (dark gray).

which is reasonable for the prototype mentioned earlier, the gain drops significantly, as shown in figures 30 and 31. In addition, there is no longer a second resonance at higher C_3 values. This behavior can be seen from a different perspective in figure 32. In terms of mathematical description, the admittance parameters of the circuit illustrated in figure 29 are given by

$$Y_{11} = -(1/(C_3C_4) + 1/(C_3C_6) + 1/(C_4C_5) + 1/(C_5C_6))/D \quad (34)$$

$$Y_{12} = (1/(C_5C_6) - 1/(C_3C_4))/D \quad (35)$$

$$Y_{21} = Y_{12} \quad (36)$$

$$Y_{22} = -(1/(C_3C_4) + 1/(C_3C_5) + 1/(C_4C_6) + 1/(C_5C_6))/D, \quad (37)$$

with

$$D = j(1/(C_3C_4C_5) + 1/(C_3C_4C_6) + 1/(C_3C_5C_6) + 1/(C_4C_5C_6))/w. \quad (38)$$

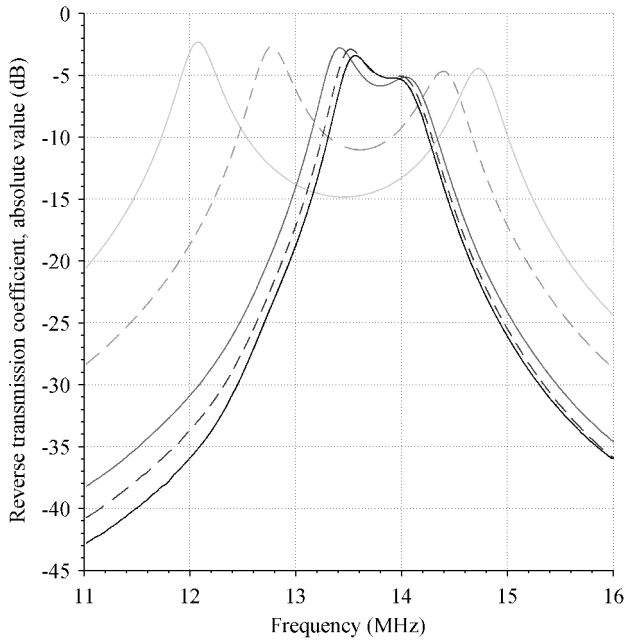

Fig. 24. Measured $|S_{12}|$ as a function of frequency for distances equal to 10 (light gray), 20, 60, 90 and 500 cm (dark gray).

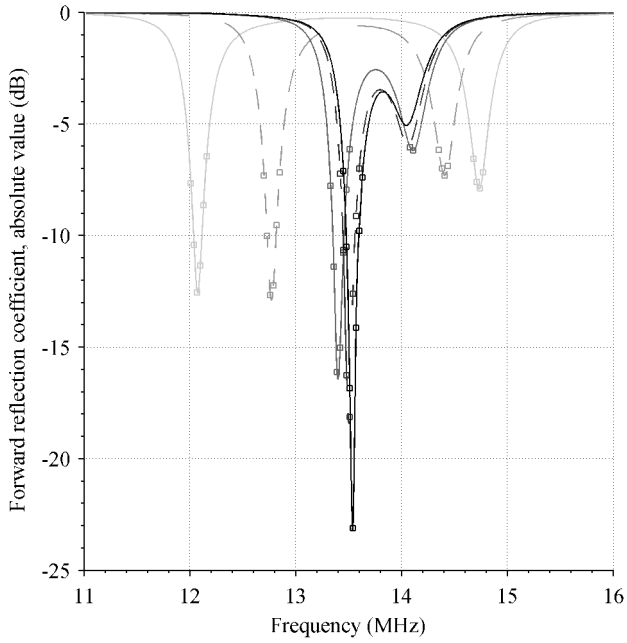

Fig. 25. Measured $|S_{11}|$ as a function of frequency for distances equal to 10 (light gray), 20, 60, 90 and 500 cm (dark gray). The experimental points are highlighted for values below -6 dB.

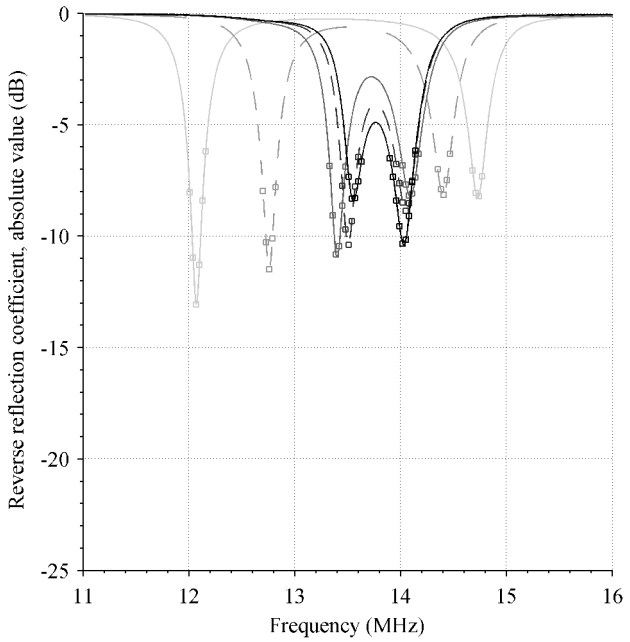

Fig. 26. Measured $|S_{22}|$ as a function of frequency for distances equal to 10 (light gray), 20, 60, 90 and 500 cm (dark gray). The experimental points are highlighted for values below -6 dB.

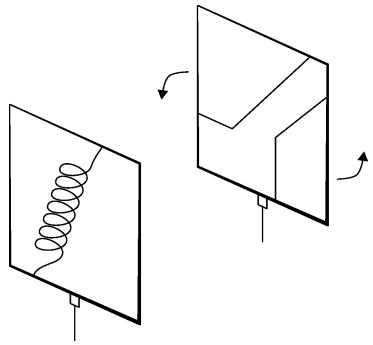

Fig. 27. Position of 0° and type of rotation used in the measurement of $|S_{21}|$ as a function of angle.

In theory, as C_5 and C_6 get closer to C_3 Y_{21} and Y_{12} tend to zero, (27) tends to zero and (16) tends to zero as well.

IV. Conclusions

One of the most interesting coupling techniques in the field of wireless power transfer is resonant magnetic coupling. This technique is very popular in the literature. In contrast, wireless power systems based on electrical coupling are quite difficult to find. As seen in this article, resonant electrical coupling has several very interesting features. The main purpose of this article was to highlight these features and demonstrate the remarkable duality that exists between resonant magnetic coupling and resonant electrical coupling. In terms of experimental results, it was not possible obtain a complete match with theory yet but some key aspects were confirmed. Future work will focus on a better characterization of resonant electrical coupling and on the possibility of constructively

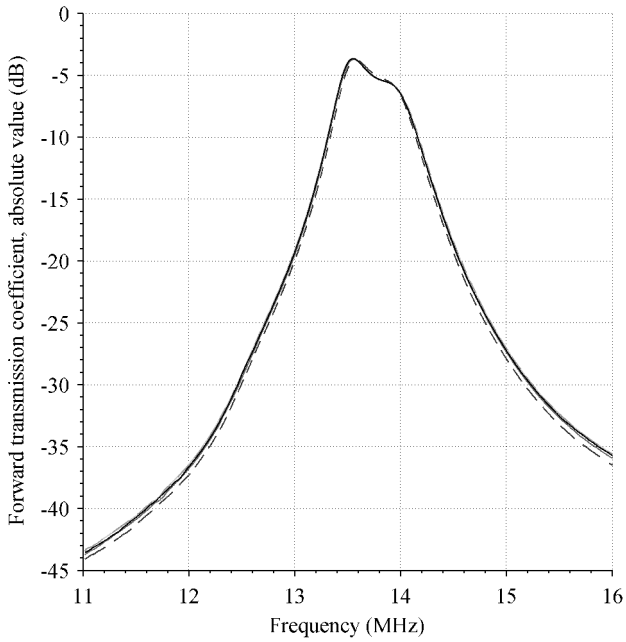

Fig. 28. Measured $|S_{21}|$ as a function of frequency for angles equal to 0 (light gray), 40, 90, 180 and 270° (dark gray) at 500 cm.

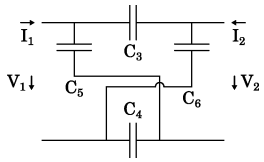

Fig. 29. Parasitic capacitances (C_5 and C_6) considered in the model presented in figure 8.

mixing the two types of coupling in order to create a hybrid coupling with improved performance. The material presented in this article extends previous publications such as [11], [12] and in particular [13].

References

[1] J.-P. Curty, M. Declercq, C. Dehollain, and N. Joehl, *Design and Optimization of passive UHF RFID Systems*. New York: Springer, 2007, ch. 2, pp. 3–4.

[2] N. Tesla, "Apparatus for transmitting electrical energy," Patent, December 1914, uS 1119732 A.

[3] W. C. Brown, "The history of power transmission by radio waves," *Microwave Theory and Techniques, IEEE Transactions on*, vol. 32, no. 9, pp. 1230–1242, September 1984.

[4] A. Kurs, "Power transfer through strongly coupled resonances," Master's thesis, Massachusetts Institute of Technology, 2007.

[5] A. Kurs, A. Karalis, R. Moffatt, J. D. Joannopoulos, P. Fisher, and M. Soljaoić, "Wireless power transfer via strongly coupled magnetic resonances," *Science*, vol. 317, no. 5834, pp. 83–86, July 2007.

[6] J. D. Joannopoulos, A. Karalis, and M. Soljaoić, "Wireless non-radiative energy transfer," Patent, July 2006, uS 7741734 B2.

[7] A. Karalis, A. Kurs, R. Moffatt, J. D. Joannopoulos, P. H. Fisher, and M. Soljaoić, "Wireless energy transfer," Patent, March 2008, uS 7825543 B2.

[8] A. P. Sample, D. A. Meyer, and J. R. Smith, "Analysis, experimental results, and range adaptation of magnetically coupled resonators for wireless power transfer," *Industrial Electronics, IEEE Transactions on*, vol. 58, no. 2, pp. 544–554, February 2011.

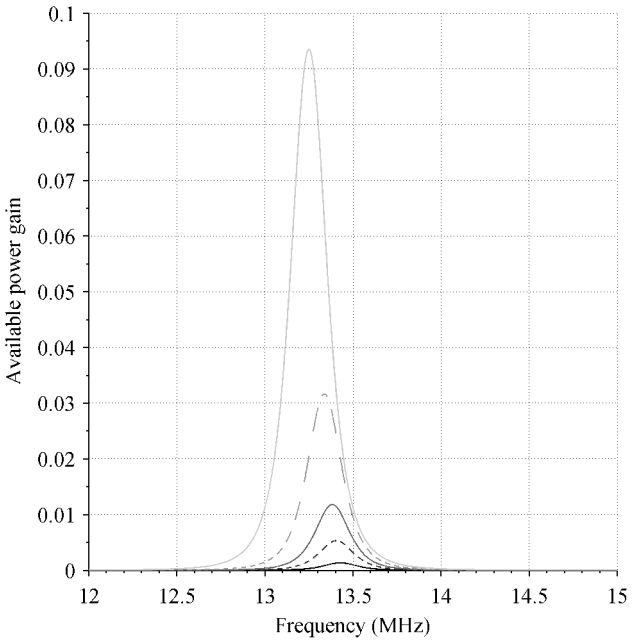

Fig. 30. Available power gain as a function of frequency for C_3 equal to 0.02 (dark gray), 0.04, 0.06, 0.1 and 0.18 pF (light gray) with C_5 and C_6 set to 70% of C_3.

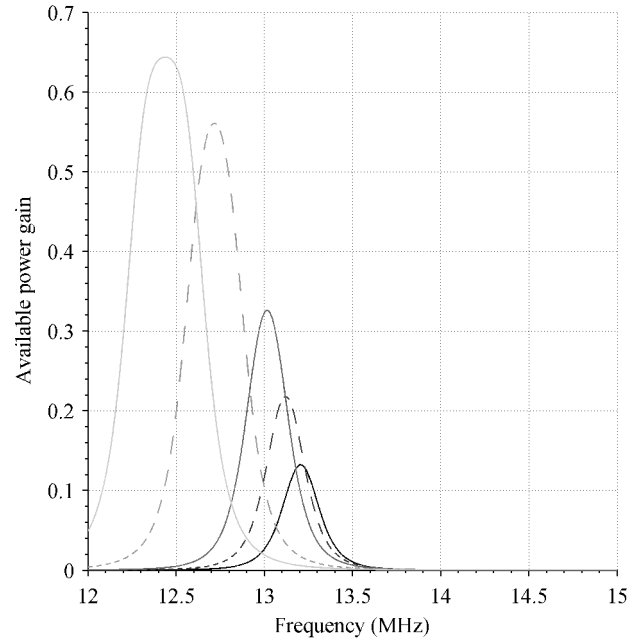

Fig. 31. Available power gain as a function of frequency for C_3 equal to 0.22 (dark gray), 0.3, 0.4, 0.7 and 1 pF (light gray) with C_5 and C_6 set to 70% of C_3.

[9] J. R. Smith and A. P. Sample, "Wireless power transfer apparatus and method thereof," Patent, April 2010, uS 2010/0187913 A1.

[10] A. P. Sample, B. H. Waters, S. T. Wisdom, and J. R. Smith, "Enabling seamless wireless power delivery in dynamic environments," *Proceedings of the IEEE*, vol. 101, no. 6, pp. 1343–1358, June 2013.

[11] K. Ichikawa and H. Bondar, "Power transfer system," Patent, August 2012, uS 2012/0299392 A1.

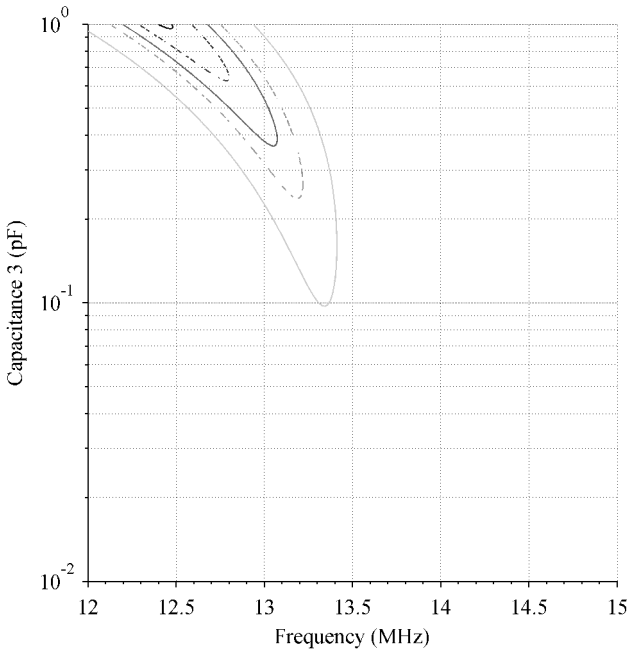

Fig. 32. Available power gain as a function of frequency and C_3 using contour lines drawn at 0.03 (light gray), 0.15, 0.29, 0.52 and 0.64 (dark gray) with C_5 and C_6 set to 70% of C_3.

[12] C. Yang and K. Tsunekawa, "Analysis and performance improvement of independent electric coupled resonance wpt system with impedance transformer," in *Wireless Power Transfer Conference (WPTC), 2014 IEEE*, May 2014, pp. 239–242.

[13] R. Fernandes, J. Matos, and N. Carvalho, "Behavior of resonant electrical coupling in terms of range and relative orientation," in *Wireless Power Transfer Conference (WPTC), 2014 IEEE*, May 2014, pp. 118–121.